# Microscopic probing of two-photon fluorescence for cancer diagnosis

For decades, molecular fluorescence-based microscopic methods have been a standard tool for wide-ranging biological applications[1]. Many molecules within the live cell (e.g. amino acids like tryptophan and tyrosine, riboflavins, nicotinamides, etc.) are fluorescent by themselves, and therefore are potential candidates to be probed using fluorescence microscopy. This phenomenon of intrinsic fluorescence is known as 'auto-fluorescence'. Amongst various fluorescence-based imaging techniques, multi-photon fluorescence microscopy[2,3] has been shown to be an excellent candidate for quantitative auto-fluorescence detection. Recently, it has been demonstrated that multi-photon excited auto-fluorescence can be a significant marker for cancer[4,5]. Here we describe the salient features of a multi-photon fluorescence microscope constructed in our laboratory and report its potential applications in cancer diagnosis.

If we use an optically thick (~20 μm) specimen, we observe both in- and out-of-focus fluorescence, which leads to a blurring of the images. This is taken care of by putting a pinhole at the *con*jugate *focal* plane and thereby effectively collecting the fluorescence arising from focal plane only, known as (one-photon) *confocal* fluorescence microscopy[6]. One can also consider fluorescence generation by an alternative excitation scheme where two (or three) photons, having half (or one-third) the energy of the single photon absorbed[2,3], are simultaneously absorbed. Although the possibility of such a process was predicted way back in 1930 (ref. 7), the practical demonstration came only after 30 years[8], with the advent of lasers as sources of intense light. This is because of the fact that the probability of such an event to occur is too low compared to one-photon absorption. This is taken care of using ultrafast lasers having pulse width ~ 100 fs, which offers gigantic instantaneous power leading to multi-photon absorption.

Due to the use of short pulses with large spectral bandwidth as well as owing to broad overlapping multi-photon absorption window of common fluorophores, simultaneous excitation of different fluorophores is common with multi-photon excitation[9]; this is in sharp contrast with one-photon excitation, where narrow-band laser lines are used to selectively excite individual fluorophores corresponding to their non-overlapping absorption maxima. Multi-photon excitation provides better axial resolution owing to complete absence of background fluorescence. Another advantage is that water is optically 'transparent' (i.e. having linear absorption coefficient of $10^{-4}$ or less) over the near infrared (NIR) wavelength region (750–1100 nm), which renders two-photon excitation with better penetration depth within biological samples; which has allowed deep-tissue imaging[10]. This motivated us to implement multi-photon fluorescence microscopy as a diagnostic tool for cervical pre-cancers, one of the commonest forms of cancer in India, by probing the intrinsic auto-fluorescence from fixed normal and malignant human tissue samples.

Among different body fluorophores, reduced nicotamide adenine dinucleotide (phosphate) (NAD(P)H) as well as flavin adenine dinucleotide (FAD) are particularly useful for two-photon auto-fluorescence (TPAF) imaging[11]. At 730 nm, the two-photon absorption cross-section of NAD(P)H is ~0.04 GM, whereas that of FAD is ~0.08 GM (1 GM = $10^{-50}$ $cm^4s$/photon-molecule)[12]. This, coupled with the fact that the fluorescence quantum yield of these fluorophores is too low (<0.1%), demands much higher power levels at the sample. The onset of cancer is marked by enhanced cellular metabolism due to tumour growth. Consequently, the elevation of these two metabolites (and hence the fluorescence from them) is a hallmark of carcinogenesis; these two fluorophores have been shown to significantly differ in concentration in normal and malignant cells[12]. A recent study on breast-cancer detection by the TPAF technique also concluded elevated level of NADH in cancer cells[13].

However, quite recently, it has been found by various studies that for cancer cell a different metabolic pathway is followed in which NADH is rather consumed to produce lactate (as is common under anaerobic conditions, i.e. in the absence of oxygen), even in the presence of abundant oxygen and is known as 'aerobic glycolysis' or 'Warburg effect'[14–16]. Thus NADH level is indeed lessened in cancer cells compared with normal cells. The reported elevated TPAF signal in cancer cells[11–13] may be due to other cellular metabolites, e.g. porphyrin derivatives which are also potential cancer markers[17]. Also, the broad emission spectra of NADH and FAD (emission maxima around 460 and 520 nm respectively) are difficult to separate from other endogenous emissions, including longer wavelength (~630 nm) fluorescence from porphyrin derivatives.

In what follows, we present a case study of using quantitative TPAF microscopy as a promising diagnostic tool in the detection of cervical pre-cancers, without any specific assignment of the origin of the difference in auto-fluorescence. We demonstrate that the optical sectioning capabilities by deep-tissue penetration as well as simultaneous excitation of many endogenous fluorophores offered by TPAF turn out to be useful in cancer diagnosis.

Transverse, fresh tissue sections were obtained from normal and abnormal biopsies in a 10-patient study. The bulk tissue was cut into small thin sections of 20 μm each using standard tissue-cutting machine (Leica Inc.). The slices were put on microscope slides and covered with a cover slip; care was taken not to trap any air bubbles. The specimens were excited with ~180 fs pulses (from mode-locked Ti : sapphire laser, Mira 900F pumped by Verdi 5, Coherent Inc.) centred on 730 nm at 100 mW time-averaged power. Images were taken using a commercial confocal microscope system (FV300 scan-head coupled with IX71 inverted microscope, Olympus), which was converted to a multi-photon type. For each sample, an axial scanning at 1 μm step-size was performed, which allowed us to get slice images as shown in Figure 1. Thus, a total of 21 sliced images were collected for each sample. Each slice image is of 235 μm × 235 μm size. Since fluorescence varies at different regions within a tissue sample, we collected the total fluorescence obtained by summing up the fluorescence intensity of each of these slices. Since tissue properties also vary from location to location within a patient, for every patient we analysed 10 samples (five normal and five malignant), each 20 μm thick and analysed similarly by slice imaging.

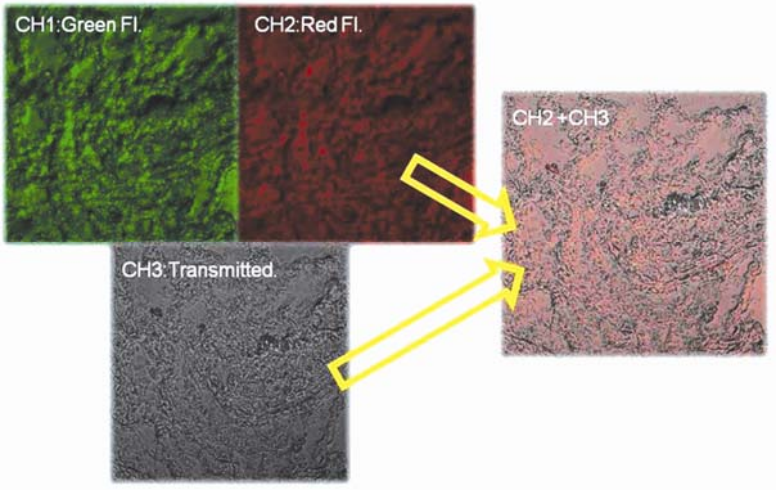


**Figure 1.** Two-photon auto-fluorescence images (slice images) of a patient suffering from cervical cancer. Channel-1 collects fluorescence in the range 400–570 nm, channel-2 in the 570–680 nm range and channel-3 collects the transmitted light. Superimposition of all the images reveals how the intrinsic fluorophores are distributed over the morphology.

| Patient No. | $T_{fi(N)}$ | $T_{fi(AB)}$ |
|---|---|---|
| 1) | 359±89 | 678 ± 77 |
| 2) | 398±45 | 423±69 |
| 3) | 562±101 | 789±105 |
| 4) | 413±82 | 582±95 |
| 5) | 608±105 | 806±123 |
| 6) | 254±46 | 432±67 |
| 7) | 669±155 | 548±164 |
| 8) | 847±208 | 1006±316 |
| 9) | 752±303 | 962±358 |
| 10) | 1056±78 | 1298±87 |

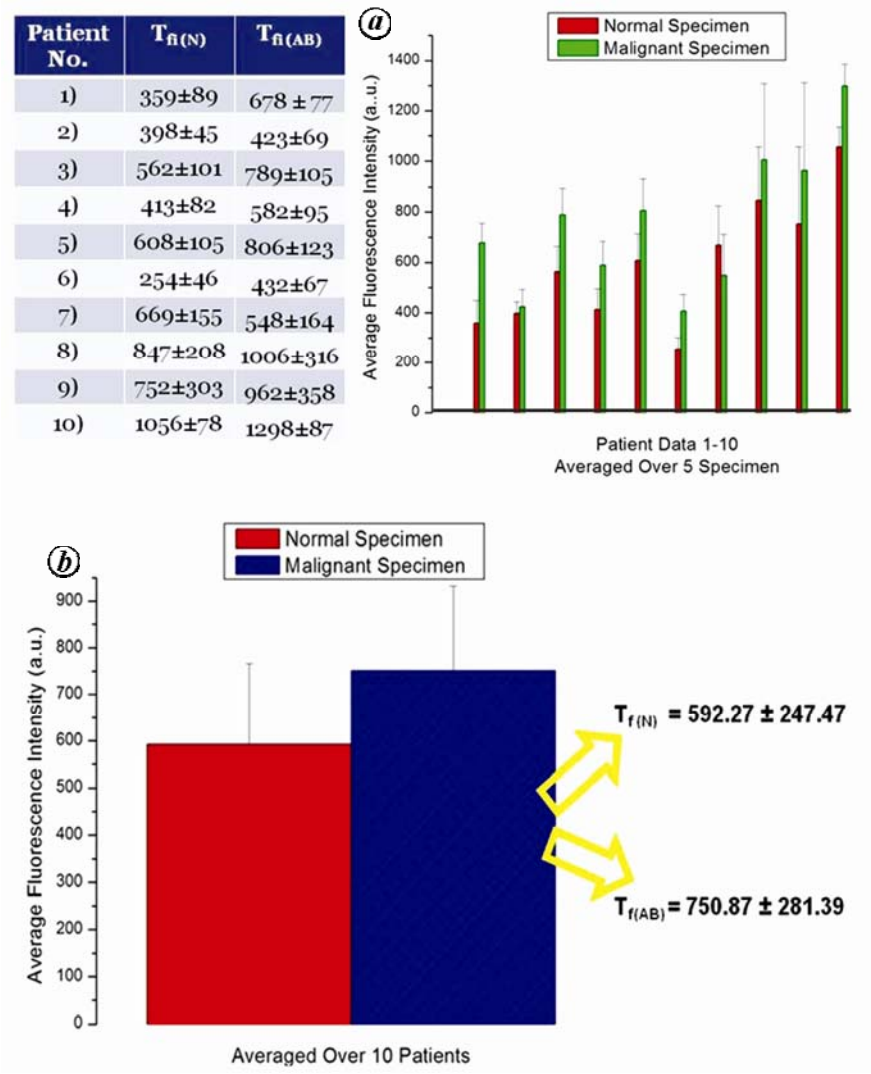


**Figure 2.** ***a***, Histograms showing average two-fluorescence intensity for 10 patients along with standard deviation (tabulated on the left panel). ***b***, Average histogram for all 10 patients.

The image analysis was carried out in standard ImageJ Freeware package (www.imagej.org). The mean intensities from all the images corresponding to different layers (or slices) within a sample were calculated and added to get total fluorescence ($T_f$) content of the sample. For every patient, fluorescence from five normal and five malignant tissue samples was measured to get the average total fluorescence ($T_{fi}$) for normal ($T_{fi(N)}$) as well as malignant ($T_{fi(AB)}$) cases, and a histogram with standard deviation was plotted (using MS Excel). This was repeated for all the 10 patients. Finally, all the $T_{fi(N)}$ and $T_{fi(AB)}$ were averaged over all 10 patients and histogram with standard deviation was plotted. Figure 2 *a* shows histograms for average fluorescence intensity for all the 10 patients. The histograms show different amounts of average TPAF intensity for normal and malignant specimens, which is usually higher in the case of malignant specimen (except patient no. 6 termed as 'outlier'). However, the normal/malignant fluorescence ratio is different for different patients, which can be attributed to the various grades of cancer (adenomatous, carcinomas, low- and high-grade dysplasia) for different patients as well as the variations due to different tissue morphologies. Figure 2 *b* shows average histogram for all 10 patients with $T_{fi(N)}$ = 592.27 ± 247.47 compared to $T_{fi(AB)}$ = 750.87 ± 281.39. Although the standard deviation is too high (247.47/592.27 for normal vs 281.39/750.87 for malignant) to conclusively use these data for prediction, they clearly reveal the elevated auto-fluorescence signal in malignant tissues compared with normal tissues.

In summary, we have described the working principle of a multi-photon fluorescence microscopy and shown its potential use in diagnosis of cervical cancer. There is a significant difference in TPAF yield in normal versus malignant tissues. However, the use of higher power levels in the experiment can be avoided by 'non de-scanned' collection set-up (where the fluorescence is collected using a dichromatic mirror placed just beneath the objective) capable of signal acquisition at much lower power levels. The reason for this large standard deviation is due to the limited number of patients; however, to have a meaningful study it is necessary to analyse samples from patients with the same ethnic origin, habitat and lifestyle, as done in the

present study. In fact, the standard deviation for NADH concentration in normal and malignant breast tissues by TPAF has been found to be quite large (99 ± 37 and 168 ± 49 μm) as studied by others[13]. Further studies with more specimens of varying parameters (e.g. age group, stage of malignancy, etc.) for standardizing the present method prior to having a real clinical application are presently being pursued in our laboratory.


1. Lakowicz, J. R., *Principles of Fluorescence Spectroscopy*, Springer, 2005.
2. Denk, W. *et al.*, *Science*, 1990, **248**, 73–76.
3. Maiti, S. *et al.*, *Science*, 1997, **275**, 530–532.
4. Bird, D. K. *et al.*, *Cancer Res.*, 2005, **65**, 8766–8773.
5. Konig, K. and Riemann, I., *J. Biomed. Opt.*, 2003, **8**, 432–439.
6. Minsky, M., *Scanning*, 1988, **10**, 128–138.
7. Göppert-Mayer, M., *Ann. Phys.*, 1931, **9**, 273–294.
8. Kaiser, W. and Garret, C. G. B., *Phys. Rev. Lett.*, 1961, **7**, 229–231.
9. Xu, C. *et al.*, *Proc. Natl. Acad. Sci. USA*, 1996, **93**, 10763–10768.
10. Centonze, V. E. and White, J. G., *Biophys. J.*, 1998, **75**, 2015–2024.
11. Huang, S. *et al.*, *Biophys. J.*, 2002, **82**, 2811–2825.
12. Palmer, G. M. *et al.*, *Photochem. Photobiol.*, 2003, **78**, 462–469.
13. Heiden, M. G. V. *et al.*, *Science*, 2009, **324**, 1029–1033.
14. Kroemer, G. and Pouyssegur, J., *Cancer Cell Rev.*, 2008, **13**, 472–482.
15. Kaelin Jr, W. B. and Thompson, C. B., *Nature*, 2010, **465**, 562–564.
16. Yu, Q. and Heikal, A. A., *J. Photochem. Photobiol. B: Biol.*, 2009, **95**, 46–57.
17. Masilamani, V. *et al.*, *J. Lumin.*, 2004, **109**, 143–154.


ACKNOWLEDGEMENTS. We thank Wellcome Trust Foundation, UK, and MCIT and DST, India for funding. A.K.D. thanks CSIR, New Delhi for graduate fellowship. We are grateful to Drs Asha Agarwal, Sudeep Thakur and Sonal, Kanpur GSVM Medical College, for providing the specimens and Prashant Shukla, Dharitri Rath and Dr Aseema Pradhan, IIT Kanpur for help in using their tissue-fixation facilities. We also thank Aditya Gupta and Vivek Bansal for their help.

Received 22 September 2009; revised accepted 2 December 2010

ARIJIT KUMAR DE[1,2]
NIKHIL N. MUTYAL[1,3]
DEBABRATA GOSWAMI[1,*]

[1]*Department of Chemistry,*
*Indian Institute of Technology,*
*Kanpur 208 016, India*
[2]*Present address:*
*Physical Bioscience Division,*
*Lawrence Berkeley National Laboratory*
*and Department of Chemistry,*
*University of California at Berkeley,*
*Berkeley, California 97420, USA*
[3]*Present address:*
*Department of Biomedical Engineering,*
*Northwestern University,*
*Evanston, IL, USA*
**For correspondence.*
*e-mail: dgoswami@iitk.ac.in*

# Cloning, overexpression, purification and characterization of maltooligosyltrehalose synthase from a cyanobacterium, *Anabaena* 7120

Trehalose is a non-reducing sugar with low energy (1 kcal $mol^{-1}$), withstands 100°C and is functional in the pH range 3.5–10 (ref. 1). Therefore, it is used as a stabilizer and preservative of foodstuff, cryoprotectant for cells in medicine, in cosmetics and various biotechnological purposes[2]. It has also been reported as a signalling molecule of higher plants[3–5], and plays an important role in *Mycobacterium tuberculosis*–host interactions[6] and in Huntingdon's and Alzheimer's diseases[7,8]. There are five types of trehalose biosynthetic pathways reported in various organisms[1]. One of the pathways having maltooligosyltrehalose synthase (MTSase) (*all0167*) and maltooligosyltrehalose trehalohydrolase (MTHase) (*all0168*) enzymes has superiority in trehalose production (up to 80–92%) in many bacteria[2]. A gene cluster constituting trehalose biosynthesizing enzymes, MTSase and MTHase, along with trehalase (*all0168*), has been reported in *Anabaena* 7120 (ref. 9) and is maximally expressed in *Anabaena* 7120 exposed to 150 mM NaCl (refs 10, 11). In addition, increase in trehalose yield may be achieved through manipulation of such enzymes.

The MTSase gene was PCR-amplified and cloned in pGEM-T Easy vector (Promega) and sub-cloned in pET-19b (Novagen) expression vector. The recombinant was transformed in *Escherichia coli* BL21 (DE3) and expressed optimally in isopropyl β-D-1 thiogalactopyranoside (IPTG) (1 mM)-induced cultures (14 h, 28°C). The recombinant MTSase enzyme purified by $Ni^{+2}$-NTA affinity chromatography showed maximum transglycosylation activity at pH 6 (40°C), with maltohexaose as the substrate. To our knowledge, there are no other reports on the expression, purification and characterization of MTSase from a cyanobacterium.

*Anabaena* 7120 was grown in BG-11 medium[12] free from combined N-source under continuous tungsten plus fluorescent illumination (14.40 $Wm^{-2}$) at 28 ± 1°C. *E. coli* NM was used as the host for vectors. The amino acid sequence of MTSase of *Anabaena* 7120 was compared with MTSase from different microbes. Protein sequence databases (Swiss_Port, PIR and GenBank) were searched using the standard search algorithm, BLASTP (NCBI, NIH). The sequences were aligned and a phylogenetic tree was generated based on the neighbour-joining (NJ) algorithm using Clustal X[13].

Genomic DNA from *Anabaena* 7120 was isolated using Marmur method[14]. PCR-amplified *all0167* from the genomic DNA using primers was designed from the nucleotide sequence (http://bacteria.kazusa.or.jp/cyanobase; GenBank accession code, Q8ZOD1). The forward primer (5′ GCG CAT ATG CGA ATT CCT AAA GCT AC 3′) and reverse primer (5′ GCG GGA TCC **TTA** TTC GGC GAT TAA CAG G 3′) contained the restriction